Defect detection in colored texture surfaces using Gabor filters

by

Du-Ming Tsai, Chih-Ping Lin, Kuo-Tang Huang

Department of Industrial Engineering and Management
Yuan-Ze University, Taiwan, R.O.C.

Corresponding author:

Du-Ming Tsai
Department of Industrial Engineering & Management
Yuan-Ze University
135 Yuan-Tung Road
Nei-Li, Tao-Yuan
Taiwan, R.O.C.

Tel: 886-3-463-8800
Fax: 886-463-8907
E-mail: iedmtsai@saturn.yzu.edu.tw

Defect detection in colored texture surfaces using Gabor filters

ABSTRACT

This paper presents a Gabor filtering approach for automatic inspection of defects in colored texture surfaces. It can simultaneously measure both chromatic and textural anomalies in an image. Two chromatic features derived from the $CIE-L*a*b*$ color space are used to form a complex number for color pixel representation. The proposed method is based on the energy response from the convolution of a Gabor filter with the color image characterized by two chromatic features in the form of a complex number. The Gabor filtering process converts the difficult defect detection in a colored texture image into simple threshold segmentation in the filtered image. Experimental results from a number of colored texture surfaces such as textile fabric, wood and tile have shown the effectiveness of the proposed method.

Key words: Surface inspection, Defect detection, Colored textures, Gabor filters

1. INTRODUCTION

1.1 Automated Visual Inspection

Image analysis techniques are being increasingly used to automate industrial inspection. The manual activity of inspection can be subjective and highly dependent on the experience of human inspectors. For defect inspection in complicated material surfaces, color and texture are two of the most important properties. Detecting various classes of defects in colored texture images is difficult using conventional gray-level imaging techniques. In this paper, a Gabor filtering scheme is proposed to tackle the problem of defect detection in colored texture images. The proposed scheme can simultaneously measure both color and textural anomalies in an image.

In automatic surface inspection, small surface defects which appear as local anomalies embedded in a homogeneous texture must be reliably detected. The class of homogeneous texture presents a self-similar pattern everywhere in the image. Many industrial materials such as textile fabrics and machined surfaces fall in this category. The proposed method can be applied to both structural and statistical textures. However, the textured surfaces to be inspected must contain periodical, repetitive patterns.

The inspection task in this paper is classified as qualitative inspection [1] which involves detecting non-quantitatively measurable but obvious faults such as scratches, stains, shedding of fibers and other ill-defined anomalies. A defect is usually small in size with respect to the imaged area, and breaks the homogeneity of the textural

pattern. Many of these unanticipated defects with color and structural anomalies cannot be described by explicit measures, making automatic defect detection difficult.

1.2 Previous Work

Most of the defect detection systems are carried out in gray-level images. Thresholding or edge detection techniques are employed to detect defects in nontextured surfaces such as glass panels [2], sheet steel [3], and uniform web materials [4]. Defects in these images can be detected easily because commonly used measures usually have very distinct values. For complicated textured surfaces in gray-level images, gray-level co-occurrence matrix methods [5, 6] in the spatial domain and Fourier transform methods [7] in the frequency domain are commonly used to describe textural features.

The Fourier-based methods characterize the spatial-frequency distribution of textured images, but they do not consider the information in the spatial domain and may overlook local deviations. In the recent past, Gabor filters were well recognized as a joint spatial/spatial-frequency representation for analyzing textured images containing highly specific frequency and orientation characteristics [8]. Gabor filter-based methods have been successfully applied to texture classification and segmentation [9, 10]. Two main methods have been proposed in the literature for selecting Gabor filters: the filter-bank approach and the filter-design approach [11]. In filter-bank approaches [12-14], the input image is generally filtered by a family of Gabor filters tuned to several resolutions and orientations. The Gabor filter bank is usually reported with frequency bandwidth in octaves and orientation bandwidth in 45 degrees. These limited parameter values are not necessarily optimal for a particular

processing task. In filter-design approaches [9, 15-17], only one or a few filters for a particular application are designed in an effort to reduce the computational burden of filter-bank approaches. The selection of the best filters is generally based on *a priori* knowledge of the textural properties derived from a spectral Fourier analysis. Clausi and Jernigan [18] gave a thorough comparison of various Gabor filter implementations for texture analysis. Classical Gabor filters consider only the gray-level information in a textured image. They do not exploit chromatic properties of textures and may fail in defect detection.

Traditional texture analysis methods are inappropriate for colored texture images because they ignore chromatic information. Since color images contain more information per pixel, color machine vision has been an active field during the last few years in agricultural applications such as color inspection of potatoes [19] and grading of oranges [20], and in industrial inspection applications such as ceramic tiles [21], granite [22], leather [23], cotton fiber [24], integrated circuits [25], and LCD panels [26].

In the analysis of color images, the description of image regions has been performed mainly using color histograms [21, 27]. However, color histograms lose the spatial information of a texture, and are not sufficient to detect small local variation in defects. More sophisticated color imaging methods have been developed for colored object recognition, colored texture classification and segmentation. Healey and Slater [28] used moments of color distributions for colored object recognition. Gevers and Smeulders [29] analyzed and developed a set of color features which are invariant to changes in viewing direction, object geometry and illumination. They achieved object recognition by histogram matching of the

selected color features. Suen and Healey [30] used color features defined by the parameters of conditional Markov fields, and employed the Mahalanobis distance to classify the color texture classes. Van de Wouwer [31] studied the colored texture classification problem using the wavelet multiresolution decomposition. Texture features are given by wavelet covariance signatures which contain the energy of each color plane and the cross correlation between different color planes. Zugaj and Lattuati [32] presented an approach for color image segmentation by a fusion between both edge pixels and region-growing images. Campadilli *et al*. [33], and Verikas *et al*. [34] addressed the color image segmentation problem using neural networks. Liu and Yang [35], and Panjwani and Healey [36] presented Markov random field models for colored texture segmentation. The model parameters were estimated using a maximum pseudo-likelihood scheme or a relaxation process.

1.3 Overview of the Proposed Scheme

Traditional color imaging methods are more concerned with the problem of image segmentation than with problems arising in defect inspection in colored texture surfaces, where local defects exhibit no distinct textural properties. This paper considers the issue of designing a single Gabor filter to detect unpredictable defects in a colored texture surface. Classical Gabor filtering schemes only take into account the gray levels of pixels. The proposed method incorporates the Gabor filter with chromatic features of pixels to detect both color and structural anomalies in a periodically textured image. Owing to the inherent limitation of Gabor filtering, the orientation of a structural texture surface under inspection is assumed to be aligned or known in advance.

In this study, two brightness-invariant chromatic features derived from the $CIE-L*a*b*$ color space [37] are used to form a complex number for colored pixel representation. The $CIE-L*a*b*$ transform is given by

$$L* = 116(Y/Y_n)^{1/3} - 16$$
$$a* = 500\left[(X/X_n)^{1/3} - (Y/Y_n)^{1/3}\right]$$
$$b* = 200\left[(Y/Y_n)^{1/3} - (Z/Z_n)^{1/3}\right]$$

where X, Y and Z are transformed from the RGB space by

$$\begin{bmatrix} X \\ Y \\ Z \end{bmatrix} = \begin{bmatrix} 0.607 & 0.174 & 0.200 \\ 0.299 & 0.587 & 0.114 \\ 0.000 & 0.066 & 1.116 \end{bmatrix} \begin{bmatrix} R \\ G \\ B \end{bmatrix}$$

X_n, Y_n and Z_n are the tristimulus values of the reference white, and can be derived from the XYZ space with (R, G, B) = (255, 255, 255) in an 8-bit display system. $L*$ is a correlate to perceived lightness. The $a*$ and $b*$ dimensions correlate approximately with red-green and yellow-blue chroma perceptions.

The proposed color Gabor filtering scheme convolves a Gabor filter with the color image characterized by two chromatic features in the form of a complex number. The design objective for the best Gabor filter is based on the minimization principle that finds the minimum energy response of a faultless textured pattern in the training process. By defining a non-negative response amplitude, each regular texture region defined in a neighborhood window will have the response amplitude close to zero, and any irregular defect region will have a distinctly high response amplitude in the filtered image. The proposed scheme then converts the difficult defect inspection in a colored texture image into simple threshold segmentation in the filtered image.

This paper is organized as follows: Section 2 first describes the classical Gabor filtering scheme in gray-level images. The proposed color Gabor filtering scheme that incorporates the classical Gabor transform with two chromatic features is then discussed. Section 3 presents the experimental results from a variety of colored textures including textile fabric, wood and tile surfaces. The paper is concluded in Section 4.

2. GABOR FILTER DESIGN

2.1 Gabor filtering in gray-level images

The 1-D Gabor function was first defined by Gabor [38], and later extended to 2-D by Daugman [8]. A 2-D Gabor filter is an oriented complex sinusoidal grating modulated by a 2-D Gaussian function, which is given by

$$G_{\sigma,\phi,\theta}(x,y) = g_{\sigma}(x,y) \cdot \exp[2\pi j\phi(x\cos\theta + y\sin\theta)] \tag{1}$$

where

$$g_{\sigma}(x,y) = \frac{1}{2\pi\sigma^2}\exp[-(x^2+y^2)/2\sigma^2], \text{ and } \quad j = \sqrt{-1}$$

The frequency and orientation of the span-limited sinusoidal grating are given by ϕ and θ, respectively. $g_{\sigma}(x,y)$ is the Gaussian function with scale parameter σ. In this study, the symmetric Gaussian function is adopted for defect detection applications. For more complicated texture patterns, asymmetric Gaussian function may be needed. The parameters of a Gabor filter are, therefore, given by the frequency ϕ, the orientation θ and the scale σ.

The Gabor filter $G_{\sigma,\phi,\theta}(x,y)$ forms a complex valued function. Decomposing $G_{\sigma,\phi,\theta}(x,y)$ into real and imaginary parts gives

$$G_{\sigma,\phi,\theta}(x,y) = R_{\sigma,\phi,\theta}(x,y) + jI_{\sigma,\phi,\theta}(x,y) \tag{2}$$

where

$$R_{\sigma,\phi,\theta}(x,y) = g_{\sigma}(x,y)\cdot\cos[2\pi\phi(x\cos\theta + y\sin\theta)]$$

$$I_{\sigma,\phi,\theta}(x,y) = g_{\sigma}(x,y)\cdot sin[2\pi\phi(x\cos\theta + y\sin\theta)]$$

The Gabor-filtered output of a gray-level image $f(x,y)$ is obtained by the convolution of the image with the Gabor filter $G_{\sigma,\phi,\theta}(u,v)$, i.e.

$$\int_{-\infty}^{\infty}\int_{-\infty}^{\infty} f(x+u, y+v)\cdot G_{\sigma,\phi,\theta}(u,v)dudv \tag{3}$$

Given a neighborhood window of size $W\times W$ with $W = 2k+1$, the discrete convolutions of $f(x,y)$ with respective real and imaginary components of $G_{\sigma,\phi,\theta}(x,y)$ are

$$G_R(x,y|\sigma,\phi,\theta) = \sum_{\ell=-k}^{k}\sum_{m=-k}^{k} f(x+\ell, y+m)\cdot R_{\sigma,\phi,\theta}(\ell,m) \tag{4.a}$$

and

$$G_I(x,y|\sigma,\phi,\theta) = \sum_{\ell=-k}^{k}\sum_{m=-k}^{k} f(x+\ell, y+m)\cdot I_{\sigma,\phi,\theta}(\ell,m) \tag{4.b}$$

Define the energy $E(x,y|\sigma,\phi,\theta)$ at (x,y) within the window $W\times W$ as

$$E(x,y|\sigma,\phi,\theta) = G_R^2(x,y|\sigma,\phi,\theta) + G_I^2(x,y|\sigma,\phi,\theta) \tag{5}$$

Note that the convolution of an image with the Gabor filter defined in eq.(3) is based on the single gray-level information. Some textured defects can only be detected in color images. The proposed Gabor filtering scheme is extended from gray-level texture images to colored texture images so that both chromatic and structural patterns of a texture can be simultaneously evaluated. The chromatic features in color images are derived from the $CIE-L*a*b*$ color space.

2.2 Gabor filtering in color images

The $CIE-L*a*b*$ color space described previously in Section 1 can also be represented in terms of the cylindrical coordinates that provide predictors of hue h_{ab} and chroma C^*_{ab} as expressed below:

$$h_{ab} = \tan^{-1}(b*/a*)$$
$$C^*_{ab} = (a^2* + b^2*)^{1/2}$$

In this study, we use only chromatic features h_{ab} and C^*_{ab} in the $CIE-L*a*b*$ space for defect detection so that the effect of changes in illumination intensity can be minimized. In gray-level images, the single gray-level information $f(x,y)$ is used for the Gabor filtering transform. In color images, two selected chromatic features $f_1(x,y)$ and $f_2(x,y)$ of each color pixel (x,y) are used to form a complex number $f_1(x,y) + j\, f_2(x,y)$, where the first chromatic feature $f_1(x,y)$ is the real part and the second chromatic feature is the imaginary part. Therefore, the complex number associated with the two chromatic features in the $CIE-L*a*b*$ space is given by $h_{ab} + j \cdot C^*_{ab}$. In this way, two chromatic features of a color image can be considered simultaneously with a sole Gabor filter.

The filtered output of a color image defined by $f_1(x,y) + j\, f_2(x,y)$ is obtained by the discrete convolution of the color image with the Gabor filter $G_{\sigma,\,\phi,\theta}(x,y)$, i.e.,

$$C(x,y) = \sum_l \sum_m \left[f_1(x+l, y+m) + j\, f_2(x+l, y+m) \right] \cdot G_{\sigma,\phi,\theta}(l,m) \tag{6}$$

The convoluted output $C(x,y)$ is also a complex number containing the real component $C_R(x,y|\sigma,\phi,\theta)$ and the imaginary component $C_I(x,y|\sigma,\phi,\theta)$. For a neighborhood window of size $W \times W$ with $W = 2k+1$, C_R and C_I are given by

$$C_R(x,y\,|\,\sigma,\phi,\theta) = \sum_{l=-k}^{k} \sum_{m=-k}^{k} \left\{ \left[f_1(x+l, y+m) \cdot R_{\sigma,\phi,\theta}(l,m) \right] - \left[f_2(x+l, y+m) \cdot I_{\sigma,\phi,\theta}(l,m) \right] \right\} \tag{7}$$

and

$$C_I(x,y\,|\,\sigma,\phi,\theta) = \sum_{l=-k}^{k} \sum_{m=-k}^{k} \left\{ \left[f_1(x+l, y+m) \cdot I_{\sigma,\phi,\theta}(l,m) \right] + \left[f_2(x+l, y+m) \cdot R_{\sigma,\phi,\theta}(l,m) \right] \right\} \tag{8}$$

where $R_{\sigma,\phi,\theta}(l,m)$ and $I_{\sigma,\phi,\theta}(l,m)$ are the same as those defined in eq. (2).

Note that eq. (6) uses two chromatic features $f_1(x,y)$ and $f_2(x,y)$ in color images, rather than the single gray-level feature $f(x,y)$ in gray-level images, so that both chromatic information and spatial information of a colored texture image are simultaneously considered in the filtering process. The energy $E_c(x,y|\sigma,\phi,\theta)$ at (x,y) of a filtered color image within the window of size $W \times W$ is defined by the squared modulus of $C(x,y)$, i.e.,

$$E_c(x,y|\sigma,\phi,\theta) = C_R^{\,2}(x,y|\sigma,\phi,\theta) + C_I^{\,2}(x,y|\sigma,\phi,\theta) \tag{9}$$

The energy defined in eq. (9) is a non-negative real number, and has a minimum value of zero. If the Gabor-filter parameters are selected so that the corresponding energy is a minimum for a specific faultless texture sample, every subimage that has a textured pattern similar to the training sample will generate an energy value close to

zero. Any subimage with a textured pattern different from the training sample will yield a distinctly large energy value since only the textured pattern resembling the training one will have an ideal objective value of zero. This process converts the difficult defect detection problem in colored texture images into a simple threshold segmentation problem in non-texture images where low energy represents homogeneous textures and high energy represents local anomalies.

In this study, we are considering a supervised inspection problem, i.e., the representative sample of a faultless colored texture is given to help in designing the most discriminating filter. Supervised systems are most appropriate for controlled circumstances in industry. The training sample can be arbitrarily selected from a faultless region of the colored texture image. The neighborhood window $W \times W$ is selected so that the representation of self-similarity of a homogeneous texture pattern is sufficient. The self-similarity means that all subimages of a textured image are similar to each other, regardless of their positions in the image. For a given training image T_0 with the size $W \times W$ and the center at (x_0, y_0), the optimal Gabor-filter parameters are given by

$$\min \ E_c(x_0, y_0 | \sigma, \phi, \theta)$$

subject to

$$\sigma_{\min} \le \sigma \le \sigma_{\max} \tag{10.a}$$

$$\phi_{\min} \le \phi \le \phi_{\max} \tag{10.b}$$

$$0 \le \theta \le 180 \tag{10.c}$$

where $E_c(x_0, y_0 | \sigma, \phi, \theta)$ is the energy of the training sample T_0 and can be

obtained from eq. (9). Note that the selected size $W \times W$ of the training image T_0 must be sufficiently large to contain the periodicity and self-similarity properties of the reference texture in question. The constraints (10.a), (10.b) and (10.c) specify the possible ranges of filter parameters σ, ϕ and θ, respectively. $\sigma_{\min}$ and $\sigma_{\max}$ are the minimum and maximum values of σ. $\phi_{\min}$ and $\phi_{\max}$ give the minimum and maximum values of the frequency parameter ϕ, and they can be set to $\phi_{\min} = 1$ and $\phi_{\max} = W$ (the width of the neighborhood window). The orientation parameter θ is restricted to the interval between $0°$ and $180°$ since symmetry makes the other directions redundant.

The formulated model above is a nonlinear constrained programming problem with multiple continuous variables. It may need sophisticated optimization techniques such as the simulated annealing (SA) search algorithm [39] to determine the best parameter values of σ, ϕ and θ. An empirical study has been conducted to compare the detection results from the exhaustive search with the resolution of 1 (i.e., integer values) and the SA search algorithm with a step size of 0.01 for all three parameters. The detection results showed that the energy function defined in eq. (9) is not very sensitive to minor variation of the parameter values. Both exhaustive and SA search methods have performed equally well for generating an objective function value smaller than 0.01. The exhaustive search with the suggested resolution setting can be implemented easily, and is computationally simple. Since the training process can be carried out off-line, a simple exhaustive search with the resolution of 1 for all three parameters will sufficiently find a best Gabor parameter set (σ, ϕ, θ).

In the inspection process, the selected Gabor filter of a given size will slide over

the whole sensed image on a pixel-by-pixel basis so that the corresponding energy of every pixel in the image can be calculated. The filter will give a small output amplitude close to zero when the sliding window covers a homogeneous texture region in the image, and will generate a large response for a discrepant region. This process transforms texture discrimination into detectable filter output.

3. EXPERIMENTAL RESULTS

In this section, we present the experimental results from a variety of colored texture images to evaluate the performance of the proposed color Gabor-filtering method. All experiments were implemented on a personal computer using the C language. The RGB images are 256×256 pixels wide with eight bits of intensity per band. The size of the neighborhood window is 65×65 pixels for all test samples, unless otherwise specified. In the training process, a subimage of size 65×65 pixels is arbitrarily selected from each faultless reference image to determine the best filter parameters. To visually display the output energy $E_c(x, y|\sigma, \phi, \theta)$ as an intensity function, the magnitude of energy is linearly converted to an 8-bit intensity. The brightness of intensity is proportional to the magnitude of energy.

3.1 Detection from Color and Gray-level Images

The chromatic features evaluated in the experiments are $h_{ab} + j \cdot C_{ab}^{*}$ derived from the $CIE - L^*a^*b^*$ color space. Figures 1(a) and 1(b) show a faultless textile fabric and a defective version of the fabric, respectively. The anomaly in Figure 1(b) is a color defect. Its structure is similar to the regular texture pattern, which makes

the defect hardly visible in the gray-level image, as seen in Figure 1(c). Figure 1(d) visually shows the output energy from the chromatic features $h_{ab} + j \cdot C_{ab}^{*}$ as an intensity function, where brightness is proportional to the magnitude of energy. It shows that all pixels in the homogeneous texture region yield small energy values close to zero, while pixels in the defective region generate relatively large energy values. The trained parameters (σ, ϕ, θ) for Figure 1(a) are (12, 1, 129) with a minimum objective value of 0.000000. Figure 1(c) demonstrates the gray-level version of the colored fabric image shown in Figure 1(b). When only the gray-level information is used in the detection process, the resulting output energy (eq. (5)) generates noise and cannot reliably detect the defect, as seen in Figure 1(e). Figure 2 presents the plot of the energy function in 3-D perspective based on the result from the chromatic features $h_{ab} + j \cdot C_{ab}^{*}$. Note that in the experiment only a single training subimage of size 65×65 pixels was used to determine the Gabor parameters. The resulting energy values of pixels in the homogeneous region of a 256×256 test image are all approximate to zero. Only pixels in the defective region yield distinctly large energy values.

3.2 Effects of Illumination and Defect Sizes

In this study, two illumination-invariant chromatic features are used to construct the color Gabor-filtering scheme. The effect of changes in illumination on the detection results is demonstrated with a wood image shown in Figure 3. The anomaly on the upper-right of the image is a structural defect. A faultless subimage obtained from the wood image in Figure 3(a) is used as the reference sample for training. Wood images in Figures 3(b) and 3(c) are, respectively, the overexposed

and underexposed versions of the training image. Figures 3(d)-(f) present the detection results as an intensity function. They show that the color Gabor filter trained under a given illumination can reliably detect all defects in the images, regardless of illumination changes. Furthermore, for the less regular texture surface in the wood surface, the defect is also well detected using the proposed color Gabor-filtering method.

In order to evaluate the effect of changes in defect size, Figures 4(a)-(c) show respectively the surface images of a tile with defects of increasing size (the defect is the blue area around the center of the image). Figures 4(d)-(f) present the resulting images from the chromatic features $h_{ab} + j \cdot C_{ab}^{*}$. It can be seen from the detection results that the defects can be reliably detected, regardless of changes in defect size. Note that the color defect as small as the one shown in Figure 4(a) is also well detected in the filtered image.

3.3 Effect of Window Sizes

In this study, the size of the neighborhood window is set at 65×65 pixels. The choice of a proper window size must be large enough to contain the periodic, repetitive pattern of a homogeneous texture in question. Too small a window size causes insufficient representation of a texture pattern, whereas too large a window size increases the computational burden.

In order to study the effect of varying window sizes on the output response of energy, the textile fabric shown in Figure 1(b) is used as a test sample. In the

experiment, the window size is varied from 65×65, 53×53, 41×41 to 25×25 pixels to analyze the impact of window size on detection results. Figures 5(a) and (b) show the detection results for the larger window sizes of 65x65 and 53x53. These window sizes generate a similar energy representation of the defect. The region associated with the defect has distinctly large magnitude of energy and is highly concentrated. However, as the window sizes are reduced to 41×41 and 25×25, as seen in Figures 5(c) and (d), the detected area of the defect becomes small and distributes in a scattering manner. It is apparent from Figure 5 that an oversized window may not generate better detection, but an undersized window may overlook subtle defects. In practical implementation, a window size in the range between 50 and 60 pixels is suggested for the trade-off between detection effectiveness and computational efficiency.

4. CONCLUSIONS

In automatic surface inspection, small defects that locally break the homogeneity of a textured pattern must be detected. Analysis of defects in a wide variety of material surfaces may require simultaneous measurements in both color and texture. Traditional approaches for automatic surface inspection are limited to gray-level images. They generally compute a set of textural features in a sliding window, and search for significant local deviations in the feature values between the sensed image and the model image. Most inspection techniques that rely on high-level textural features suffer from the difficulty and time-consuming nature of extracting features from each specific textured surface.

In this paper we have presented a Gabor-filtering approach for automatic

inspection of defects in colored texture surfaces. It is designed to be highly responsive to local variations of both color and texture. The proposed method is based on the output response of energy from the convolution of a Gabor filter with the color image characterized by two chromatic features in the $CIE-L*a*b*$ space. The best parameters of the Gabor filter for a given colored texture image is selected so that the responsive energy of a homogeneous texture is approximately zero. Any regions with color and textural anomalies in the sensed image will generate distinctly large energy values and, therefore, a simple binary threshold can be selected easily to discriminate between homogeneous regions and defective regions in the filtered image. The experimental results from a number of test samples including textile fabric, wood and tile surfaces have shown the effectiveness of the proposed color Gabor-filtering defect detection method.

The proposed method is not sensitive to changes in lighting and defect size. However, due to the inherent property of 2-D Gabor filters, the proposed color Gabor filtering method is rotation-dependent for textures with oriented structure. In practical implementation, the textural surface to be inspected in a manufacturing process must be mechanically aligned. If the orientation of a structural texture is unknown before the inspection, the orientation of the dominant line pattern in the spatial domain image can be determined easily by detecting the high-energy frequency components in the Fourier domain image using a 1-D Hough transform, as proposed by Tsai and Hsieh [40]. The inspection image can then be transformed so that its orientation is coincident with that of the training sample.

REFERENCES

[1] T. S. Newman, and A. K. Jain: 'A survey of automated visual inspection', *Computer Vision and Image Understanding*, 1995, **61**, 231-262.

[2] J. Wilder: 'Finding and evaluating defects in glass', in 'Machine Vision for Inspection and Measurement', (ed. H. Freeman), 237-255, 1989, New York, Academic Press,

[3] J. Olsson, and S. Gruber: 'Web process inspection using neural classification of scattering light', Proceedings of the IEEE International Conference on 'Industrial Electronics Control': IECON'92, San Diego, 1992, 1443-1448.

[4] D. Brzakovic, and N. Vujovic: 'Designing defect classification system: a case study', *Pattern Recognition*, 1999, **29**, 1401-1419.

[5] C. Sum, and W. G. Wee: 'Neighboring gray level dependence matrix', *Computer Vision, Graphics, Image Processing*, 1982, **23**, 341-352.

[6] L. H. Siew, and R. M. Hogdson: 'Texture measures for carpet wear assessment', *IEEE Trans. Pattern Anal. Mach. Intel.*, 1988, **10**, 92-105.

[7] S.-S. Liu, and M. E. Jernigan: 'Texture analysis and discrimination in additive noise', *Computer Vision, Graphics, Image Processing*, 1990, **49**, 52-67.

[8] J. G. Daugman: 'Uncertainty relation for resolution in space, spatial-frequency, and orientation optimized by two-dimensional visual cortical filters', *J. Opt. Soc. Amer.*, 1985, **2**, 1160-1169.

[9] A. Teuner, O. Pichler and B. J. Hosticka: 'Unsupervised texture segmentation of images using tuned matched Gabor filters', *IEEE Trans. Image Process.*, 1995, **4**, 863-870.

[10] T. Randen, and J. H. Husoy: 'Filtering for texture classification: a comparative study', *IEEE Trans. Pattern Anal. Mach. Intell.*, 1999, **21(4)**, 291-310.

[11] T. P. Weldon, W. E. Higgins, and D. F. Dunn, 'Gabor filter design for multiple texture segmentation', *Optical Engineering*, 1996, **35**, 2852-2863.

[12] T. R. Reed, and H. Wechsler, 'Segmentation of textured images and Gestalt organization using spatial/spatial-frequency representations', *IEEE Trans. Pattern*

Anal. Mach. Intell., 1990, **12**, 1-12.

[13] K. R. Namuduri, R. Mehrotra, and N. Ranganathan: 'Efficient computation of Gabor filter based multiresolution responses', *Pattern Recognition*, 1994, **27**, 925-938.

[14] P. P. Rahgu, and B. Yegnanarayana: 'Segmentation of Gabor-filtered textures using deterministic relaxation', *IEEE Trans. Image Process.*, 1996, **5,** 1625-1636.

[15] A. C. Bovik, M. Clark, and W. S. Geisler: 'Multichannel texture analysis using localized spatial filters', *IEEE Trans. Pattern Anal. Mach. Intell.*, 1990, **12**, 55-73.

[16] D. Dunn, and W. E. Higgins: 'Optimal Gabor filters for texture segmentation', *IEEE Trans. Image Process.*, 1995, **4**, 947-964.

[17] T. P. Weldon, W. E. Higgins, and D. F. Dunn: 'Efficient Gabor filter design for texture segmentation', *Pattern Recognition*, 1996, **29**, 2005-2015.

[18] D. A. Clausi, and M. E. Jernigan: 'Designing Gabor filters for optimal texture separability', *Pattern Recognition*, 2000, **33**, 1835-1849.

[19] L. Zhou, V. Chalana and Y. Kim: 'PC-based machine vision system for real-time computer-aided potato inspection', *International Journal of Imaging System and Technology*, 1998, **9(6)**, 423-433.

[20] M. Recce, A. Plebe, J. Taylor and G. Tropiano: 'Video grading of oranges in real time', *Artificial Intelligence Review*, 1998, **12**, 117-136.

[21] C. Boukouvalas, J. Kittler, R. Marik and M. Petrou: 'Color grading of randomly textured ceramic tiles using color histograms', *IEEE Trans. Industrial Electronics*, 1999, **46(1)**, 219-226.

[22] K. Y. Song, J. Kittler and M. Petrou: 'Defect detection in random colour textures', *Image and Vision Computing*, 1996, **14**, 667-683.

[23] M. Tafuri, A. Branca, G. Attolico, A. Distante and W. Delancy: 'Automatic leather inspection of defective patterns', Proc. of SPIE, Bellingham, WA (1996) 108-119.

[24] Y. J. Han, Y.-J. Cho, W. E. Lambert and C. K. Bragg: 'Identification and measurement of convolutions in cotton fiber using image analysis', *Artificial Intelligence Review*, 1998, **12**, 201-211.

[25] M. Barth, D. Hirayama, G. Beni and S. Hackwood: 'A color vision inspection

system for integrated circuit manufacturing', *IEEE Trans. Semiconductor Manufacturing*, 1992, **5(4)**, 290-301.

[26] K. Nakashima: 'Hybrid inspection system for LCD color filter panels', IEEE Instrumentation and Measurement Technology Conference, 1994, 689-692.

[27] C. L. Novak, and S. A. Shafer: 'Methods for estimating scene parameters from color histograms', *Journal of the Optical Society of America A: Optics, Image Science and Vision*, 1994, **11(11)**, 3020-3036.

[28] G. Healey, and D. Slater: 'Global color constancy: recognition of objects by use of illumination invariant properties of color distribution', *Journal of the Optical Society of America A: Optics, Image Science and Vision*, 1994, **11(11)**, 3003-3010.

[29] T. Gevers, and A. W. M. Smeulders: 'Color-based object recognition', *Pattern Recognition*, 1999, **32**, 453-464.

[30] P.-H. Suen, and G. Healey: 'Modeling and classifying color textures using random fields in a random environment', *Pattern Recognition*, 1999, **32**, 1009-1017.

[31] G. van de Wouwer, P. Scheunders, S. Livens and D. van Dyck: 'Wavelet correlation signatures for color texture characterization', *Pattern Recognition*, 1999, **32**, 443-451.

[32] D. Zugaj, and V. Lattuati: 'A new approach for color images segmentation based on fusing region and edge segmentations outputs', *Pattern Recognition*, 1998, **31**,105-113.

[33] P. Campadelli, D. Medici and R. Schettini: 'Color image segmentation using Hopfield networks', *Image and Vision Computing*, 1997, **15**, 161-166.

[34] A. Verikas, K. Malmqvist and L. Bergman: 'Colour image segmentation by modular neural network', *Pattern Recognition Letters*, 1997, **18**, 173-185.

[35] J. Liu, and Y. H. Yang: 'Multiresolution color image segmentation', *IEEE Trans. Pattern Anal. Mach. Intell.*, 1994, **16**, 689-700.

[36] D. K. Panjwani, and G. Healey: 'Markov random fields for unsupervised segmentation of texture color images', *IEEE Trans. Pattern Anal. Mach. Intell.*, 1995, **17**, 939-954.

[37] M. D. Fairchild: 'Color Appearance Models', 1998, Reading, Mass., Addison

Wesley.

[38] D. Gabor: 'Theory of communication', *J. Inst. Elec. Eng.*, 1946, **93**, 429-457.

[39] D. M. Tsai, S.-K. Wu and M.-C. Chen: 'Optimal Gabor filter design for texture segmentation using stochastic optimization', *Image and Vision Computing*, 2001, **19**, 299-316.

[40] D. M. Tsai, and C.-Y. Hsieh: 'Automated surface inspection for directional textures', *Image and Vision Computing*, 1999, **18**, 49-62.

(a)

(b)

(d)

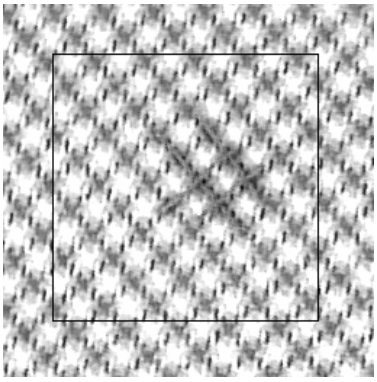

(c)

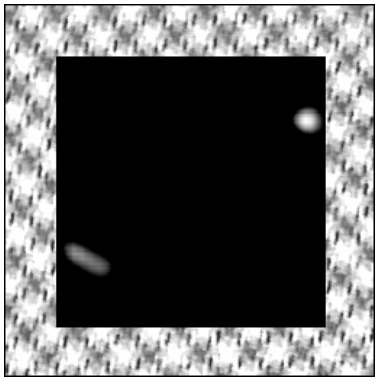

(e)

Figure 1. (a) A faultless fabric surface; (b) a defective fabric surface; (c) the gray-level image of (b); (d) visual display of the energy response as an intensity function based on the result from $h_{ab} + j \cdot C_{ab}^{*}$; (e) the detection result from the gray-level image in (c).

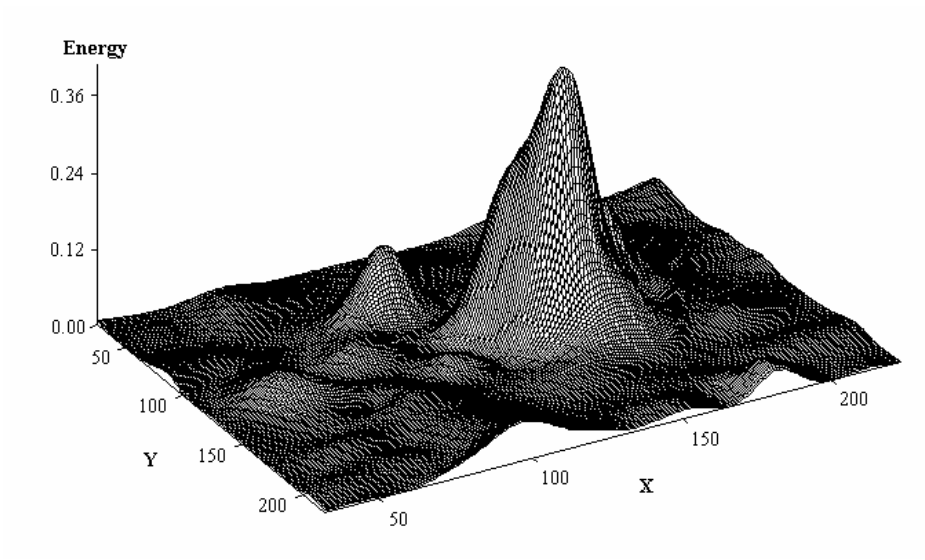

Figure 2. The energy function of Figure 1(d) in 3-D perspective based on the filtering result from $h_{ab} + j \cdot C_{ab}^{*}$.

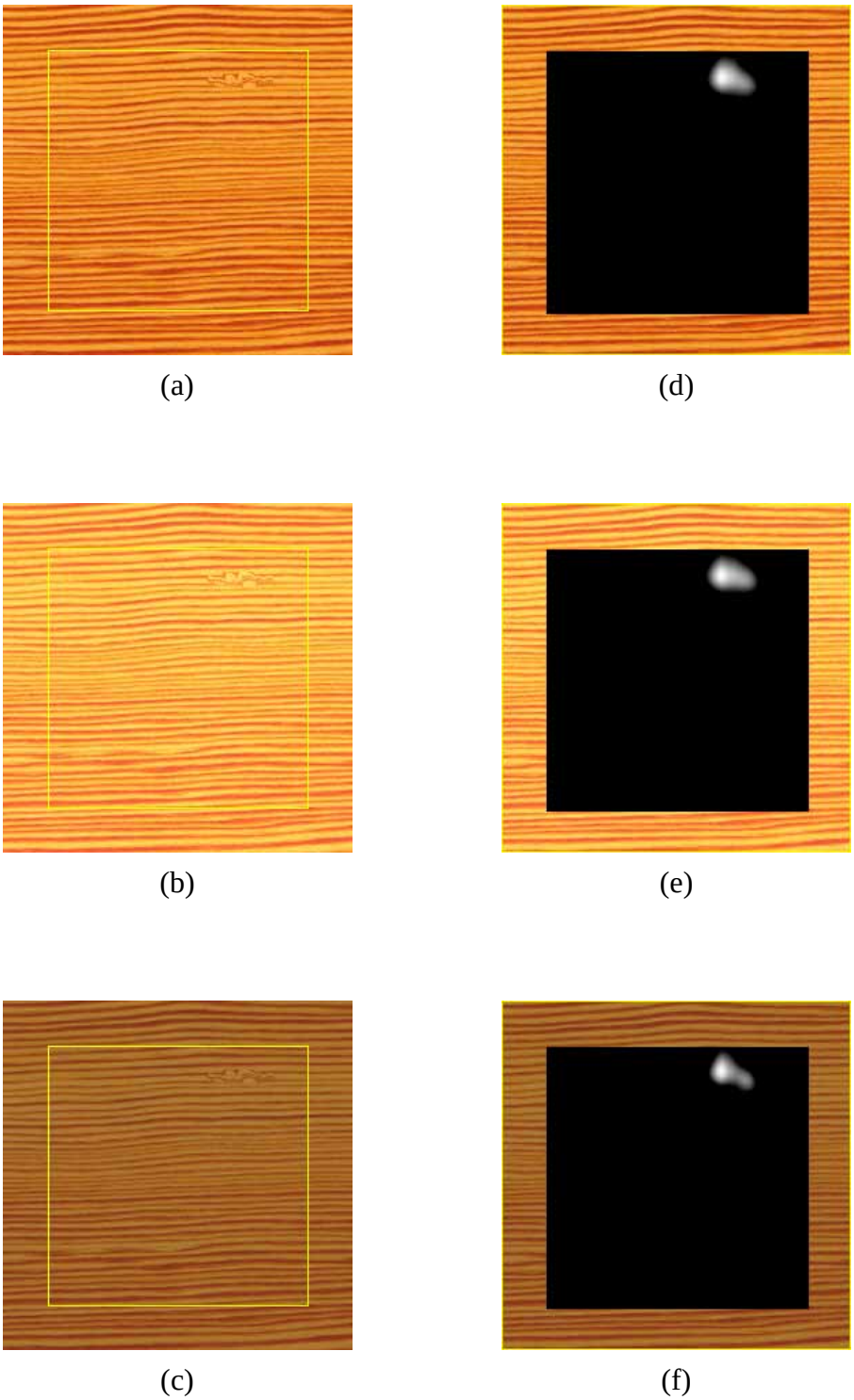

Figure 3. The effect of changes in illumination intensity: (a) the wood image used for training; (b) an overexposed image of the wood; (c) an underexposed image of the wood; (d), (e), (f) the detection results of the wood images in (a), (b) and (c), respectively.

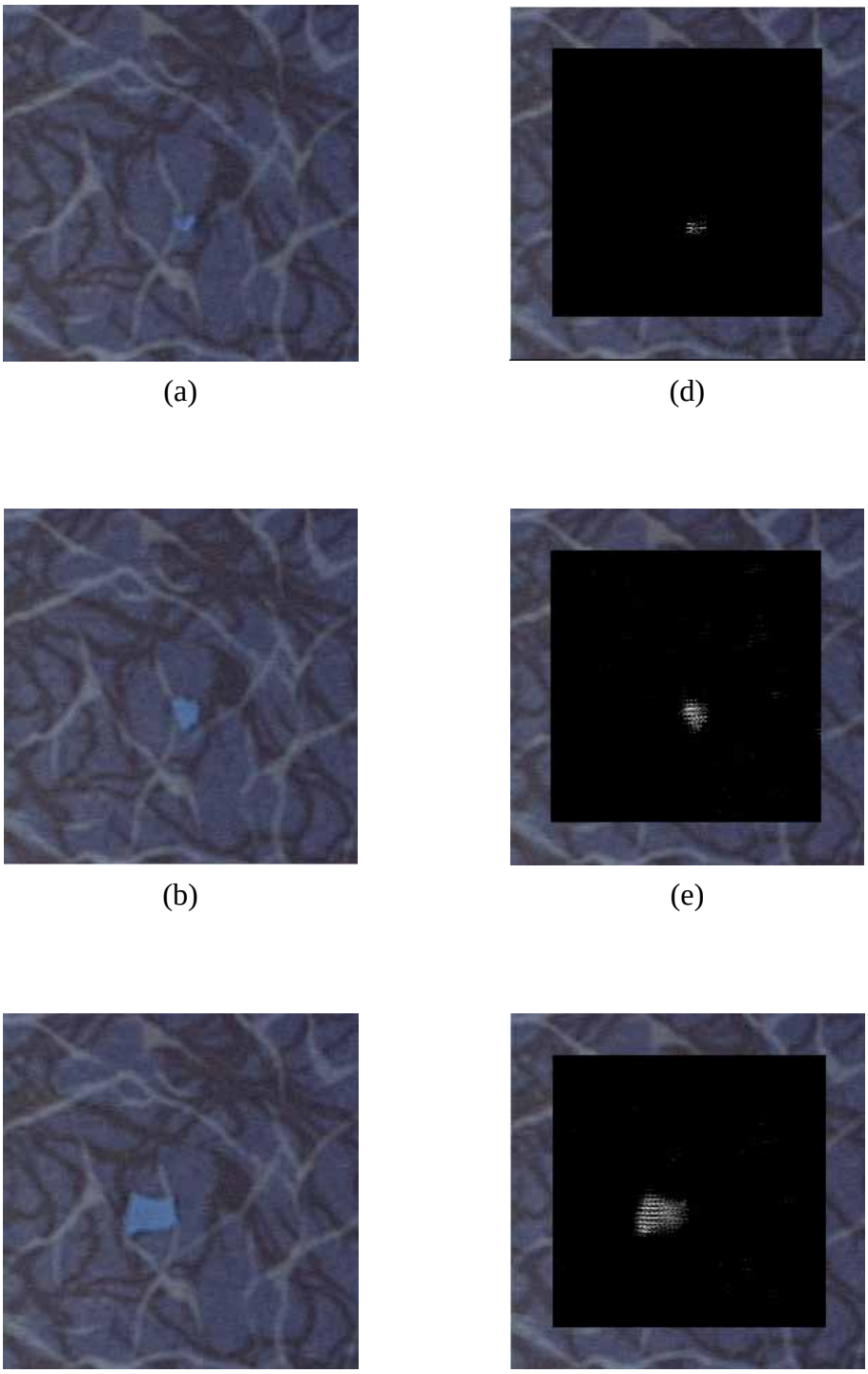

(a) (d)

(b) (e)

(c) (f)

Figure 4. The effect of changes in the defect size: (a), (b), (c) tile images with defects of increasing size; (d), (e), (f) the detection results of the tile images in (a), (b) and (c), respectively.

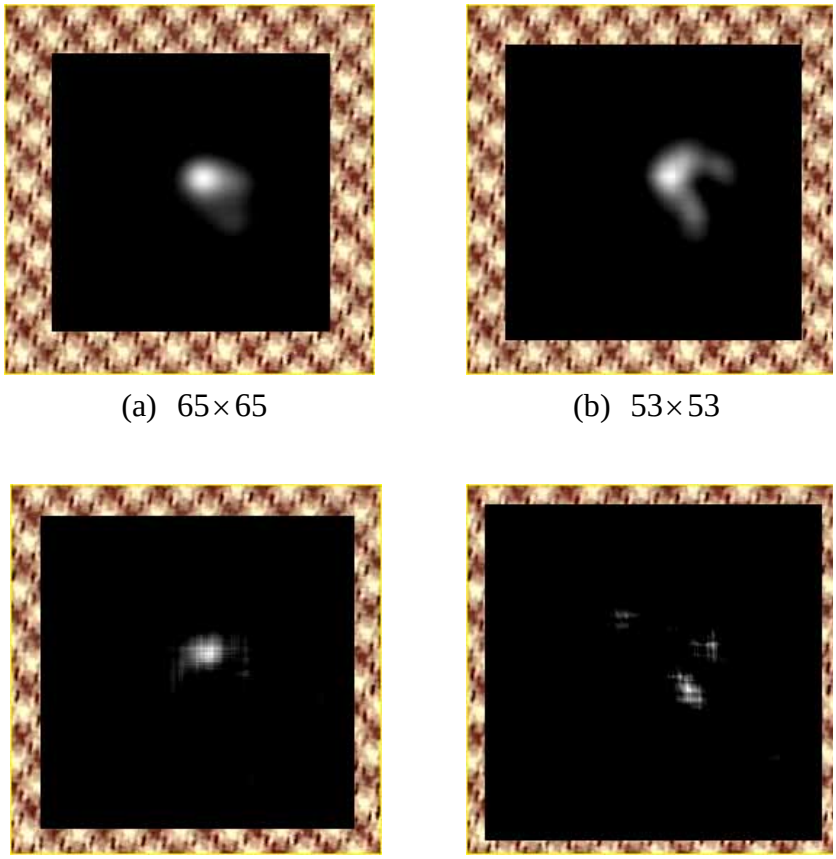

(a) 65×65 (b) 53×53

(c) 41×41 (d) 25×25

Figure 5. The effect of changes in the window size for the test sample of Figure 1(b): (a), (b), (c), (d) the detection results from window sizes 65×65, 53×53, 41×41 and 25×25 pixels, respectively.